

Estimation of Complex Permittivity of Silicon at 2.45 GHz Microwave Frequency

by

Siddharth Kulasekhar Varadan

A Thesis Presented in Partial Fulfillment
of the Requirements for the Degree
Master of Science

Approved April 2014 by the
Graduate Supervisory Committee:

Terry Alford, Co-Chair
George Pan, Co-Chair
Stefan Myhajlenko

ARIZONA STATE UNIVERSITY

May 2014

ABSTRACT

Estimation of complex permittivity of arsenic-doped silicon is the primary topic of discussion in this thesis presentation. The frequency that is of interest is 2.45 GHz, frequency typically used in conventional microwave ovens. The analysis is based on closed-form analytical expressions of cylindrical symmetry. A coaxial/radial line junction with the central conductor sheathed in dielectric material, which is As-doped silicon in this case, are analyzed. Electrical and magnetic field equations governing the wave propagation in this setup are formulated by applying the necessary boundary conditions. Input admittance is computed using the fields in the device and reflection coefficient is calculated at the input. This analytical solution is matched to the reflection coefficient acquired by experiments conducted, using VNA as the input source. The contemplation is backed by simulation using High Frequency Structural Simulator, HFSS. Susceptor-assisted microwave heating has been shown to be a faster and easier method of annealing arsenic-doped silicon samples. In that study, it was noticed that the microwave power absorbed by the sample can directly be linked to the heat power required for the annealing process. It probes the validity of the statement that for arsenic-doped silicon the heating curve depends only on its sheet properties and not on the bulk as such and the results presented here gives more insight to it as to why this assumption is true. The results obtained here can be accepted as accurate since it is known that this material is highly conductive and electromagnetic waves do not penetrate in to the material beyond a certain depth, which is given by the skin depth of the material. Hall measurements and four-point-probe measurements are performed on the material in support of the above contemplation.

DEDICATION

I would like to dedicate this to my loving and caring parents, Usha and Kulasekhar, without whom I would not have been here today, my uncle, Kasturi, who has given me anything that I would ask him of and more.

ACKNOWLEDGMENTS

I take this opportunity to express my profound gratitude to Dr. Alford for his kind support and faith he has shown in me as we rode past many ups and downs during the course of this work. I thank Dr. Pan for his timely inputs and resources to do this work.

I would like to thank Mr. Birtcher for allowing me to use his lab facilities and dedicating his time in conducting the experiments. I owe a great deal to Zhao for her help and infinite measurements she did for me whenever I asked her for a favor.

I would like to thank Dr. Aberle for sharing his knowledge on HFSS simulation software and on the subject. I wish to thank Dr. Myhajlenko for being in my committee and taking your interest in my work and evaluating it.

I would like to thank my friend, Subramanian for his guidance and for giving me this opportunity to work with Dr. Alford.

I thank all my family, friends and wellwishers who have always been there to show me the right path whenever I deviated.

This research was partially funded Intel Corporation under Grant BZ91050

TABLE OF CONTENTS

| | Page |
|---------------------------------|------|
| LIST OF TABLES | vi |
| LIST OF FIGURES | vii |
| CHAPTER | |
| 1 INTRODUCTION | 1 |
| 1.1 Ion Implantation | 1 |
| 1.2 Microwave Heating | 1 |
| 1.3 Permittivity | 2 |
| 1.4 Cylindrical Waveguide | 3 |
| 1.5 Implantation | 3 |
| 1.6 Microwave Annealing | 3 |
| 2 FORMULATION | 5 |
| 2.1 Setup | 5 |
| 2.2 Numerical Formulation | 7 |
| 3 RESULTS | 13 |
| 3.1 Experimental Findings | 13 |
| 3.1.1 Unannealed Samples | 13 |
| 3.1.2 Annealed Samples | 16 |
| 3.2 Simulation Results | 18 |
| 3.3 Analytical Results | 22 |
| 3.2 Heating Curve | 23 |

| CHAPTER | Page |
|------------------------------------|------|
| 4 DISCUSSION | 31 |
| 5 CONCLUSION AND FUTURE WORK | 36 |
| REFERENCES..... | 37 |

LIST OF TABLES

| Table | Page |
|--|------|
| 1. The dose and the dopant in each sample under consideration | 13 |
| 2. Temperature at which arsenic-doped silicon attains stability for various dose . | 28 |
| 3. Unannealed samples computed complex permittivity | 31 |
| 4. Hall measurement of arsenic-doped silicon post annealing | 32 |
| 5. Four-point-probe measurement on samples conducted post annealing | 33 |
| 6. Comparison of rate of change of temperature obtained analytically with the heating curves | 34 |

LIST OF FIGURES

| Figure | Page |
|---|------|
| 1. The model of experimental setup | 6 |
| 2. Infinite cylindrical antenna excited by magnetic frill at a width of $2h$ | 7 |
| 3. Experimental setup | 7 |
| 4. S_{11} in dB for undoped Si wafer before annealing | 14 |
| 5. S_{11} in dB for As doped Si with a dose of $1 \times 10^{15} / \text{cm}^2$ before annealing..... | 15 |
| 6. S_{11} in dB for As doped Si with a dose of $2 \times 10^{15} / \text{cm}^2$ before annealing | 15 |
| 7. S_{11} in dB for As doped Si with a dose of $4 \times 10^{15} / \text{cm}^2$ before annealing | 16 |
| 8. S_{11} in dB for As doped Si with a dose of $1 \times 10^{15} / \text{cm}^2$ after annealing | 17 |
| 9. S_{11} in dB for As doped Si with a dose of $2 \times 10^{15} / \text{cm}^2$ after annealing | 17 |
| 10. S_{11} in dB for As doped Si with a dose of $1 \times 10^{15} / \text{cm}^2$ after annealing..... | 18 |
| 11. A model of HFSS replicating the experimental setup, similar to the one shown in figure 2 and figure 3..... | 19 |
| 12. S_{11} in dB of annealed silicon wafer (for all doses) acquired from HFSS | 20 |
| 13. S_{11} in dB obtained via simulation for As doped Si unannealed sample with a dose $1 \times 10^{15} / \text{cm}^2$ | 21 |
| 14. S_{11} in dB obtained via simulation for As doped Si unannealed sample with a dose $2 \times 10^{15} / \text{cm}^2$ | 21 |
| 15. S_{11} in dB obtained via simulation for As doped Si unannealed sample with a dose $1 \times 10^{15} / \text{cm}^2$ | 22 |
| 16. S_{11} (in dB) comparison of experimental results and analytical solution for annealed silicon sample (for all dose) | 23 |

| Figure | Page |
|--|------|
| 17. Heating curve of As doped Si with dose $1 \times 10^{15} / \text{cm}^2$ | 24 |
| 18. Heating curve of As doped Si with dose $2 \times 10^{15} / \text{cm}^2$ | 25 |
| 19. Heating curve of As doped Si with dose $4 \times 10^{15} / \text{cm}^2$ | 25 |
| 20. Heating curve of As doped Si with dose $1 \times 10^{15} / \text{cm}^2$ | 26 |
| 21. Heating curve of As doped Si with dose $2 \times 10^{15} / \text{cm}^2$ | 27 |
| 22. Heating curve of As doped Si with dose $4 \times 10^{15} / \text{cm}^2$ | 27 |
| 23. Heating curve of As doped Si with silicon base for dose $1 \times 10^{15} / \text{cm}^2$ | 29 |
| 24. Heating curve of As doped Si with silicon base for dose $2 \times 10^{15} / \text{cm}^2$ | 29 |
| 25. Heating curve of As doped Si with silicon base for dose $4 \times 10^{15} / \text{cm}^2$ | 30 |

CHAPTER 1

INTRODUCTION

1.1 Ion Implantation

Semiconductor materials like silicon are doped with defects to increase its conductivity. One such process is called ion implantation, where the dopants are added to the required level deliberately. These defects are called dopants. The electromagnetic properties, such as permittivity, of the silicon are affected by such a doping. Silicon devices have been rapidly scaled down over the years which presents greater processing challenges, although the performance of the devices have been faster. Doping level needs to be increased significantly to counterbalance the effects of scaling down. Ion implantation is the most commonly used method for placing the dopants in to the silicon substrate. Several other methods, such as solid-source, in practice have been found difficult to control. Also, this method incorporates dopants upto and if necessary beyond the solid solubility level. Hence, ion implantation is controllable and reproducible [1], non-equilibrium integrated circuit (IC) process technique.

1.2 Microwave Heating

There is a drawback in using ion implantation. The implantation at such a high concentration can damage the silicon's surface layer. The depth of the damage is found to be proportional to nuclear energy loss deposited by the kinematic scattering events implanted dopants [2]. Microwave heating has been proposed in [2] as one of the methods to repair the damage created by ion implantation and to electrically activate dopants. This

presents a more uniform, volumetric heating of the wafer mainly due to the penetration depth of the microwave radiation. Hence the study of microwave heating becomes very important. In RF Heating or Microwave Heating, the material is subjected to an electromagnetic radiation which causes the molecules in the material to oscillate, thereby generating heat. This phenomenon has wide applications ranging from microwave ovens, to therapeutic medical treatment [3]. Hence, the study of microwave heating during the susceptor-assisted annealing process becomes a paramount importance.

1.3 Permittivity

One of the various factors that affect the heating curve is the complex permittivity of the material. Complex permittivity is an important electromagnetic property. In many applications such as microwave circuit designs, high speed digital circuits, packaging, *etc.* knowledge of permittivity becomes essential as it is one of the key parameter. Therefore, substantial research have been conducted towards determining the permittivity of a material [14]-[30]. Some of these measurement techniques were more prominent than the others such as, cavity resonators, transmission lines, free space and open ended coaxial probe. Relative permittivity and loss tangent measurements for FR4 dielectric material were performed by Guo in [4]. This work addressed the issues faced by Robert H. Voelker in [30], where radiation loss were ignored making the loss tangent calculation less accurate. Also, Robert H. Voelker in [30] uses rectangular parallel-plate structure to measure which has measured lineshapes closely and irregularly distributed making the data difficult to be dealt.

1.4 Cylindrical Waveguide

Keam and Williamson in [5], suggest that junctions between coaxial line and other transmission line, such as rectangular waveguide, cylindrical waveguide resonator, *etc.*, have wide applications in a variety of microwave devices. Prior to their findings, design of these devices were based on empirical knowledge. The coaxial line is considered as a radial line surrounded by homogeneous dielectric sheath.

1.5 High Frequency Structural Simulator

High Frequency Structural Simulator (HFSS) is an Ansys's commercial finite element method solver for electromagnetic structures [3]. This 3-D full wave simulation enables modeling and simulating high frequency components such as, antennas, RF/Microwave components such as filters, transmission lines and packaging. HFSS can be used for several purposes, most frequently for extracting various matrix parameters such as Scattering (S) parameters, Impedance (Z) parameters, Admittance (Y) parameters, visualizing 3-D near and far electromagnetic fields and generating full wave SPICE model.

1.6 Microwave Annealing

Heavy implantation damages the surface of silicon wafer to the extent of amorphization [8]. Repairing the damages is of paramount importance to make the films crystalline, and to electrically activate the dopants for the devices to function as desired. In [7], Rajitha and *et al.* propose susceptor-assisted annealing as a faster means of annealing. The MW ($2.8 \times 10^4 \text{ cm}^3$ cavity) oven was used for the post- anneal with single frequency 2.45 GHz

radiation generated with the use of a 1200 W magnetron source [9]. The wafer temperature was monitored with the use of a Raytek Compact MID series pyrometers.

This investigation estimates the complex permittivity of a silicon wafer via reflection coefficient method. Experiments performed were validate with the numerical and simulation results. The simulation is performed on HFSS software. The reflection coefficient from the coaxial cable was obtained and was matched with the reflection coefficient obtained from the simulation. Four samples with varying doping concentration were analyzed and presented in this paper. Sample 1 is an undoped Si substrate, sample 2, 3 and 4 has Arsenic (As) doped in the Si substrate at a varying concentration level of $1 \times 10^{15}/\text{cm}^2$, $2 \times 10^{15}/\text{cm}^2$ and $4 \times 10^{15}/\text{cm}^2$, respectively. Each wafer has a 0.5 mm laser-hole drilled completely through the wafer. Two types of microwave annealing were carried out, one susceptor-assisted annealing and the other with silicon as base. Hall measurements and four-point-probe measurements were conducted to corroborate the experimental results.

CHAPTER 2

FORMULATION

2.1 Setup

Figure 1 shows the model of the experimental setup. The coaxial cable was fed to cylindrical waveguide via an SMA connector which acts as an antenna feed, assumed as an infinite, perfectly conducting rod with radius a . This antenna was mounted on a dielectric surface. In this presentation, it was assumed that the width of the central coaxial cable extending from the bottom of the coaxial cable to the top of the cylinder is uniform. This assumption does not affect the magnitude of the S_{11} of the silicon wafer and hence will not affect the calculation of complex permittivity. The dielectric mount, extending from the inner conductor to the outer conductor, is a Teflon. The inner and outer conductor were copper. The cylindrical cavity was bound by metal on all sides hence it was assumed that the radiation was nil.

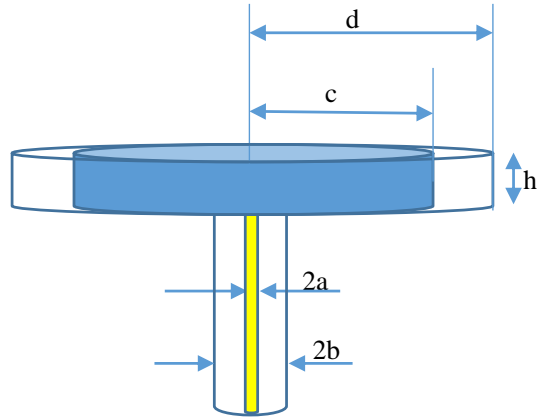


Figure 1 The model of the experimental setup

The central conductor has a radius of $r=a$, the coax cable has a radius of $r=b$. The height of the cylindrical cavity is variable and generally depends on the height of the material under test. The height of the silicon is h . The material under test, silicon, has a radius of $r=c$ and the cylindrical cavity has a radius of $r=d$. The region between $r=c$ and $r=d$ is assumed to free space. The central conductor's outer edge was assumed to touch the inner edge of the silicon which was not the case but they were so close that this assumption just. The dimensions of the coaxial cable was set such that it supports the quasi-TEM (Transverse Electromagnetic) wave mode in the required frequency of interest. All the conductors were assumed to be perfect conductors. All the waves were assumed to be axially symmetric. The fields have the time dependence of $e^{j\omega t}$. Using image theory [6], it can be demonstrated that the fields in such junctions were analogous to fields in infinite cylindrical antenna excited by infinite magnetic frills with a spacing of $2h$ as shown in figure 2. Figure 3 shows the lab setup for this experiment.

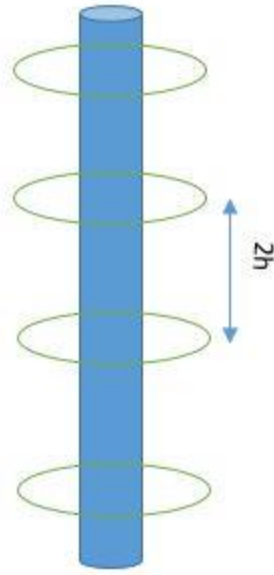


Figure 2 Infinite cylindrical antenna excited by magnetic frills at a width of $2h$



Figure 3 Experimental setup.

2.2 Numerical Formulation

Previous works carried out by Guo, *et al.* in [4] and Keam, *et al.* in [5] extensively dealt with lossless dielectric materials. In this study, the material was considered to be lossy and this assumption has been supported by the results shown in the following sections. The

field inside the cylindrical cavity resonator, E_z and H_ϕ are functions of field distribution in infinite cylindrical antenna fed by a coaxial cable as shown in equations (2.1-2.2)

$$E_z(\rho, z) = \sum_{m=-\infty}^{\infty} E_z^*(\rho, z + 2mh) \quad (2.1)$$

$$H_\phi(\rho, z) = \sum_{m=-\infty}^{\infty} H_\phi^*(\rho, z + 2mh) \quad (2.2)$$

where, $E_z^*(\rho, z)$ and $H_\phi^*(\rho, z)$ are field distribution inside infinite cylindrical antenna.

Fields can be determined by the vector potentials

$$\vec{E} = \frac{1}{j\omega\mu\epsilon} (\nabla\nabla \bullet + k^2) \vec{A} - \frac{1}{\epsilon} (\nabla \times \vec{F}) \quad (2.3)$$

$$\vec{H} = \frac{1}{\mu_0} (\nabla \times \vec{A}) + \frac{1}{j\omega\mu\epsilon} (\nabla\nabla \bullet + k^2) \vec{F} \quad (2.4)$$

The only non-zero component in electric and magnetic vector potentials \mathbf{A} and \mathbf{F} are A_z and F_ϕ , hence equations (2.3) and (2.4) can be rewritten as

$$E_z = \frac{1}{j\omega\epsilon\mu} \left(\frac{\partial^2}{\partial z^2} + k^2 \right) A_z - \frac{1}{\epsilon} \rho \frac{\partial}{\partial \rho} \rho F_\phi \quad (2.5)$$

$$H_\phi = -j\omega F_\phi - \frac{1}{\mu} \frac{\partial}{\partial \rho} A_z \quad (2.6)$$

Many prior works such as [4] and [5] have solved the equations for vector potentials in coaxial line as well as cylindrical line using Fourier transform, green's function and Maxwell's equation and have arrived at

$$A_z^*(\rho, \alpha) = \frac{\mu}{2\pi} I(\alpha) I_0(qa) K_0(q\rho) \quad (2.7)$$

$$F_{\phi}^*(\rho, \alpha) = -2\varepsilon \begin{cases} I_1(q\rho) \int_b^c e(\rho') \rho' K_1(q\rho) d\rho' & a \leq \rho \leq b \\ K_1(q\rho) \int_b^{\rho} e(\rho') \rho' I_1(q\rho') d\rho' + I_1(q\rho) \int_{\rho}^c e(\rho') \rho' K_1(q\rho') d\rho' & b \leq \rho \leq c \\ K_1(q\rho) \int_b^c e(\rho') \rho' I_1(q\rho') d\rho' & c \leq \rho \leq d \end{cases} \quad (2.8)$$

F_{ϕ}^* and A_z^* are Fourier transform of F_{ϕ} and A_z , respectively. I_l , I_0 , K_0 and K_l are Bessel functions. $\alpha = m\pi/h$, k' is the wave number inside the material under test, $q' = \sqrt{\alpha^2 - k'^2}$, ρ is distance of the point from the center of the coaxial cable. Fourier Transform of equation (2.5) and (2.6) gives,

$$E_z^*(\rho, \alpha) = \frac{\alpha}{\omega\mu\varepsilon} \frac{\partial}{\partial \rho} A_z^*(\rho, \alpha) - \frac{j\alpha}{\varepsilon} F_{\phi}^*(\rho, \alpha) \quad (2.9)$$

$$H_{\phi}^*(\rho, \alpha) = \frac{1}{\mu} \frac{\partial}{\partial \rho} A_z^*(\rho, \alpha) - j\omega F_{\phi}^*(\rho, \alpha) \quad (2.10)$$

E_z^* and H_{ϕ}^* are Fourier transformation of E_z and H_{ϕ} , respectively. Using Fourier series expansion in equations (2.1) and (2.2) E_z and H_{ϕ} can be written as,

$$E_z(\rho, z) = \frac{1}{2h} \left[E_z^*(\rho, 0) + 2 \sum_{m=1}^{\infty} E_z^* \left(\rho, \frac{m\pi}{h} \right) \cos \left(\frac{m\pi z}{h} \right) \right] \quad (2.11)$$

$$H_{\phi}(\rho, z) = \frac{1}{2h} \left[H_{\phi}^*(\rho, 0) + 2 \sum_{m=1}^{\infty} H_{\phi}^* \left(\rho, \frac{m\pi}{h} \right) \cos \left(\frac{m\pi z}{h} \right) \right] \quad (2.12)$$

Using these equations and solving for boundary conditions at $\rho=a$, $\rho=b$, $\rho=c$ and $\rho=d$ following equations were obtained for $a \leq \rho \leq b$:

$$E_z = \frac{-q'^2 \eta'}{j2\pi k'} I(\alpha) I_0(q'a) K_0(q'r) - \frac{2}{\ln(b/a)} [I_0(q'r) K_0(q'b) - I_0(q'a) K_0(q'r)] + AI_0(q'r) \quad (2.13)$$

$$H_\phi = \frac{q'^2}{2\pi} I(\alpha) I_0(q'a) K_1(q'r) + \frac{j2k'}{q' \eta' \ln(b/a)} \left[\frac{1}{q'r} - I_1(q'r) K_0(q'b) - I_0(q'a) K_1(q'r) \right] + \frac{jk'}{q' \eta'} AI_1(q'r) \quad (2.14)$$

The fields in the region between $b \leq \rho \leq c$ is:

$$E_z = \frac{-q'^2 \eta'}{j2\pi k'} I(\alpha) I_0(q'a) K_0(q'r) - \frac{2}{\ln(b/a)} K_0(q'r) \{I_0(q'b) - I_0(q'a)\} + AI_0(q'r) \quad (2.15)$$

$$H_\phi = \frac{q'^2}{2\pi} I(\alpha) I_0(q'a) K_1(q'r) + \frac{j2k'}{q' \eta' \ln(b/a)} [K_1(q'r) \{I_0(q'b) - I_0(q'a)\}] + \frac{jk'}{q' \eta'} AI_1(q'r) \quad (2.16)$$

And the fields in the region $c \leq \rho \leq d$ is:

$$E_z = E(K_0(qr) + SI_0(qr)) \quad (2.17)$$

$$H_\phi = \frac{-jk}{q\eta} E(K_1(qr) - SI_1(qr)) \quad (2.18)$$

$q = \sqrt{\alpha^2 - k^2}$ where k is the wavenumber in the air/free space. η and η' are intrinsic wave impedance of free space and material under test, respectively. The constants E and A equal

$$E = \frac{1}{S_0} \left\{ \frac{-q'\eta'}{2j\pi k'} I(\alpha) I_0(q'a) K_1(q'c) - \frac{2}{\ln(b/a)} K_0(q'c) [I_0(q'b) - I_0(q'a)] + A I_0(q'c) \right\} \quad (2.19)$$

$$A = \frac{I(\alpha) I_0(q'a) K_1(q'c) \left\{ \frac{q'^2 \eta' k S_1}{2q\eta k' S_0} - \frac{q'}{2\pi} \right\} + \frac{2j \{I_0(q'b) - I_0(q'a)\}}{\ln(b/a)} \left\{ \frac{k S_1}{q\eta S_0} K_0(q'c) - \frac{k'}{q'\eta'} K_1(q'c) \right\}}{\frac{jk'}{q'\eta'} I_1(q'c) + \frac{jk S_1}{q\eta S_0} I_0(q'c)} + \frac{\frac{jk'}{q'\eta'} I_1(q'c) + \frac{jk S_1}{q\eta S_0} I_0(q'c)}{\frac{jk'}{q'\eta'} I_1(q'c) + \frac{jk S_1}{q\eta S_0} I_0(q'c)} \quad (2.20)$$

where, $S_0 = K_0(qc) + S I_0(qc)$ and $S_1 = K_1(qc) - S I_1(qc)$. S is the variable that takes care of the surrounding in which this experiment is setup.

$$I = \frac{j4\pi k'}{q'^2 \eta' \ln(b/a)} \frac{q' S_1 (K_1(q'c) I'_{ba} - I_0(q'c) K'_{ba}) - q \epsilon S_0 (I_1(q'c) K'_{ba} + K_1(q'c) I'_{ba})}{q' S_1 (K'_0(q'c) I'_0(q'a) - I_0(q'c) K_0(q'a)) - q \epsilon S_0 (I_1(q'c) K_0(q'a) + K_1(q'c) I_0(q'a))} \quad (2.21)$$

where, $K'_{ba} = K_0(q'b) - K_0(q'a)$ and $I'_{ba} = I_0(q'b) - I_0(q'a)$.

Reflection Coefficient can be analytical obtained by calculating the input admittance of the setup. As proposed in [4] and [5] Y_{in} can be determined by,

$$Y_{in} = \frac{2\pi \int_a^b H_\phi(\rho,0)d\rho}{\ln(b/a) \int_a^b E_z(\rho,0)d\rho} \quad (2.22)$$

We assume that the excitation to be 1 V, for easier analysis, which makes equation (2.22)

$$Y_{in} = \frac{2\pi}{\ln(b/a)} \int_a^b H_\phi(\rho,0)d\rho \quad (2.23)$$

Using equations (2.23) and (2.14),

$$Y_1 = \frac{q'I(\alpha)}{\ln(b/a)} I_0(q'a) \{K_0(q'b) - K_0(q'a)\} \quad (2.24)$$

$$Y_2 = \frac{j4\pi k'}{q'\eta' \ln^2(b/a)} \left[\frac{1}{q'} \ln(b/a) - K_0(q'b) \{I_0(q'b) - I_0(q'a)\} - I_0(q'a) \{K_0(q'b) - K_0(q'a)\} \right] \quad (2.25)$$

$$Y_3 = \frac{j2\pi k'}{q'\eta' \ln(b/a)} A \{I_0(q'b) - I_0(q'a)\} \quad (2.26)$$

$$Y_{in} = Y_1 + Y_2 + Y_3 \quad (2.27)$$

CHAPTER 3

RESULTS

Eight samples have been considered in this investigation. Table 1 gives the details of each sample's dose, in cm^{-2} , the dopant and whether it was an annealed or unannealed sample.

| Sample # | Dopant/State | Dose (cm^{-2}) |
|----------|-----------------------------|---------------------------|
| 1 | None/Unannealed | Nil |
| 2 | None/Annealed | Nil |
| 3 | As ⁺ /Unannealed | 1×10^{15} |
| 4 | As ⁺ /Annealed | 1×10^{15} |
| 5 | As ⁺ /Unannealed | 2×10^{15} |
| 6 | As ⁺ /Annealed | 2×10^{15} |
| 7 | As ⁺ /Unannealed | 4×10^{15} |
| 8 | As ⁺ /Annealed | 4×10^{15} |

Table 1 The dose and the dopant in each sample under consideration

The results are presented in 3 parts, namely, analytical solutions, simulation results and experimental findings.

3.1 Experimental findings

3.1.1 Unannealed samples

Figure 4 shows the reflection coefficient (S_{11}) obtained for undoped sample prior to annealing. Undoped Silicon has the high reflection coefficient for frequencies 1-4 GHz

implying that it was highly conductive. Figures 5 through 7 shows the reflection coefficient of silicon wafer doped with As^+ prior to annealing with dose $1 \times 10^{15}/\text{cm}^2$, $2 \times 10^{15}/\text{cm}^2$ and $4 \times 10^{15}/\text{cm}^2$, respectively.

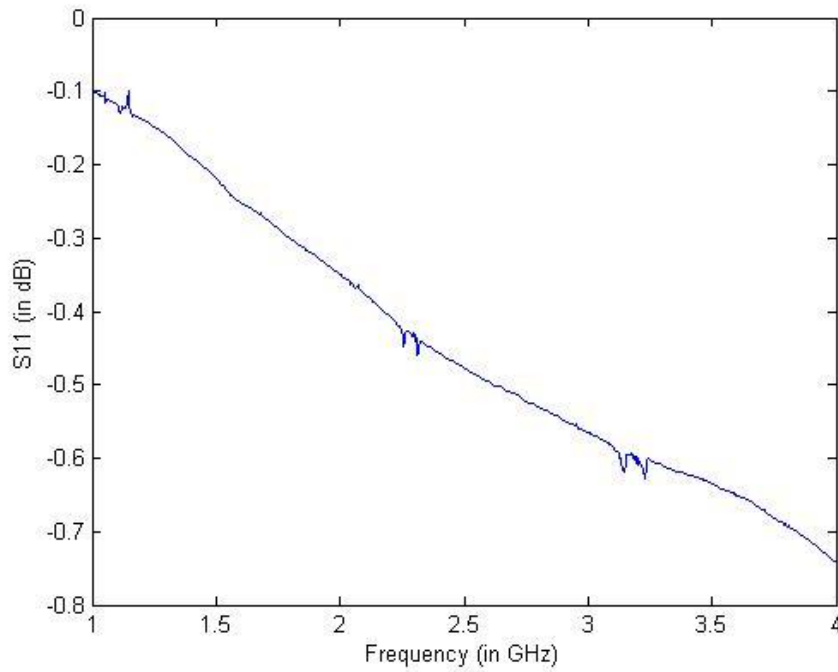


Figure 4 S11 in dB for undoped Si wafer before annealing

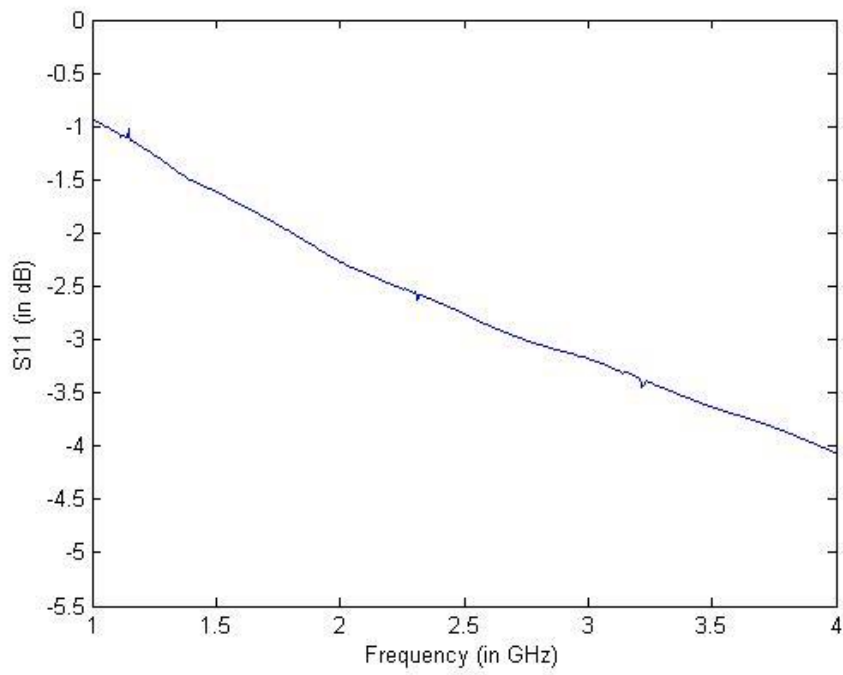


Figure 5 S11 in dB for As doped Si with a dose $1 \times 10^{15} / \text{cm}^2$ sample before annealing

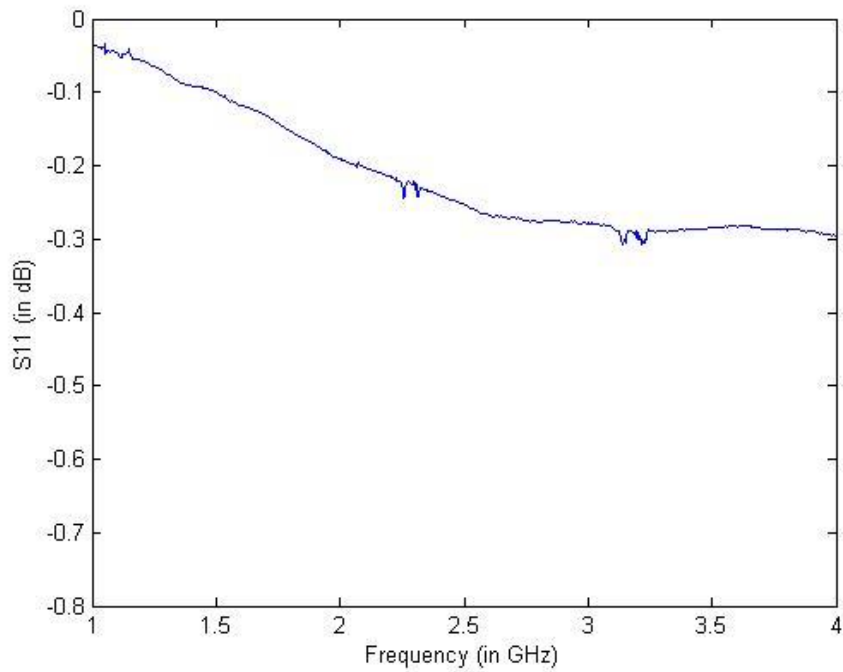


Figure 6 S11 in dB for As doped Si with a dose $2 \times 10^{15} / \text{cm}^2$ sample before annealing

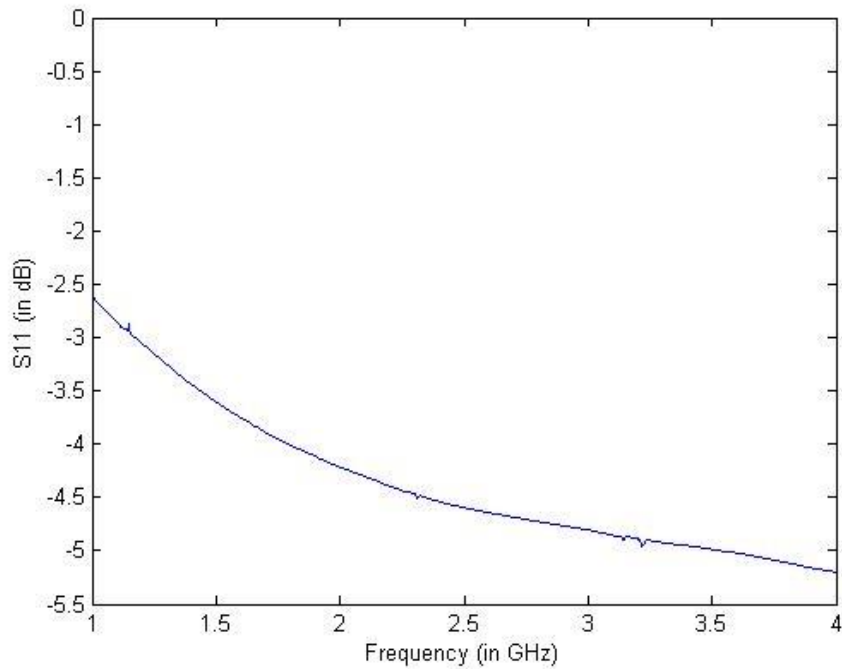


Figure 7 S11 in dB for As doped Si with a dose $4 \times 10^{15} / \text{cm}^2$ sample before annealing

The sample with dose $4 \times 10^{15} / \text{cm}^2$ has less reflection coefficient than the sample with dose $1 \times 10^{15} / \text{cm}^2$ and both have far lesser reflection than the undoped silicon, indicating that undoped silicon has high loss. However, the sample with dose $2 \times 10^{15} / \text{cm}^2$ has much more reflection, indicating very low loss. The reflection coefficient were measured as *S11* in dB

3.1.2 Annealed Samples

Figures 8-10 present the reflection coefficient obtained experimentally for annealed samples for doses $1 \times 10^{15} / \text{cm}^2$, $2 \times 10^{15} / \text{cm}^2$ and $4 \times 10^{15} / \text{cm}^2$, respectively.

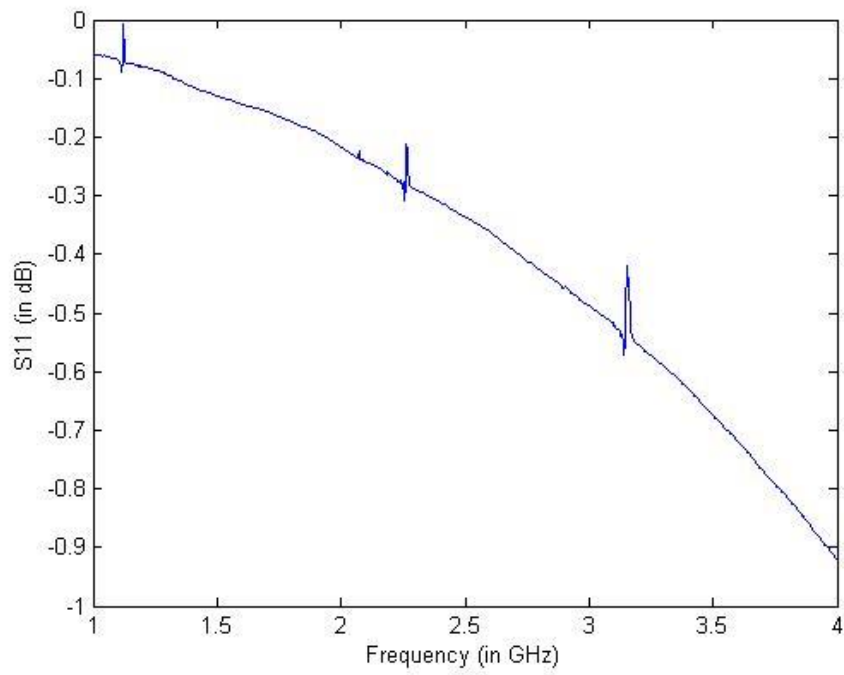


Figure 8 S11 in dB for As doped Si with a dose $1 \times 10^{15} / \text{cm}^2$ post annealing

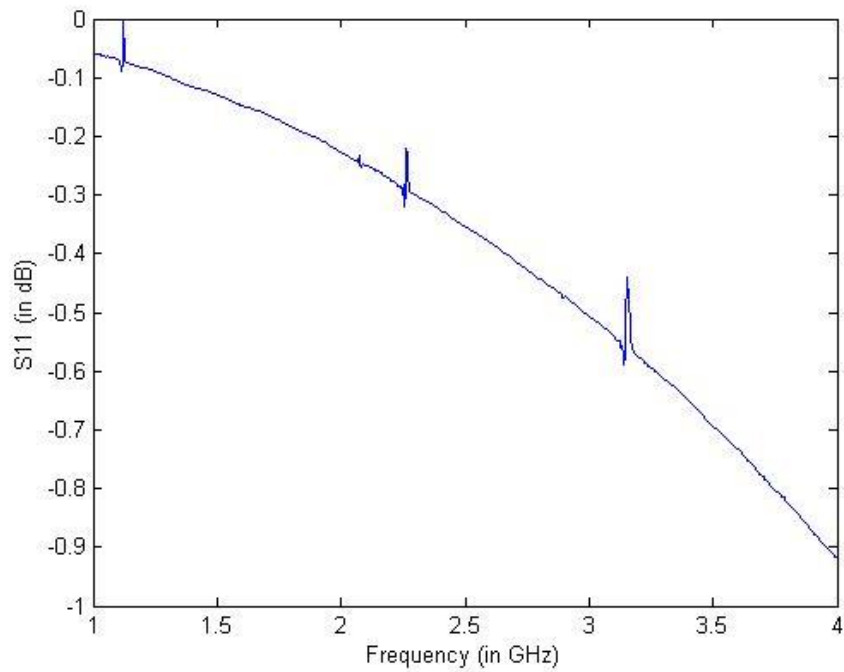


Figure 9 S11 in dB for As doped Si with a dose $2 \times 10^{15} / \text{cm}^2$ sample post annealing

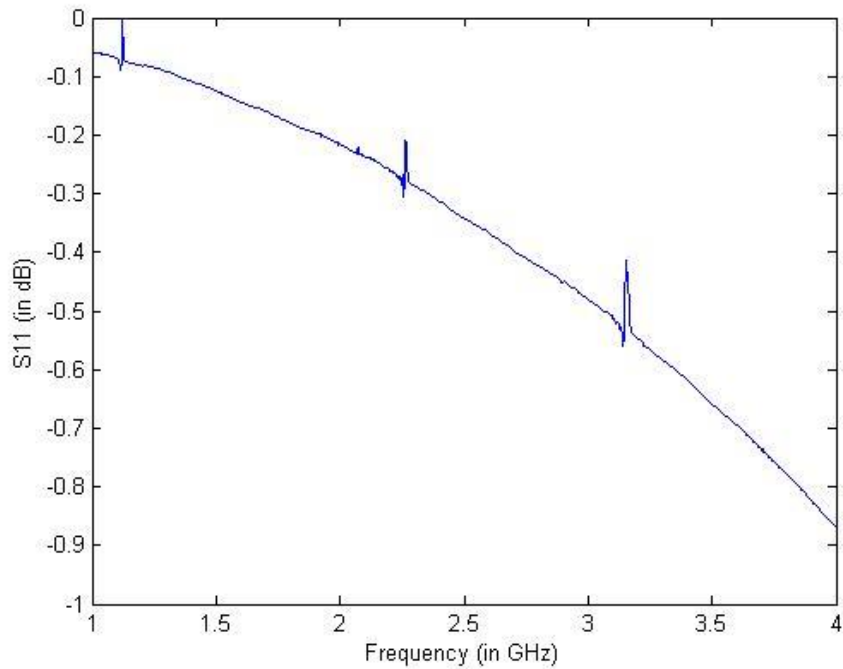


Figure 10 S11 in dB for As doped Si with a dose $4 \times 10^{15} / \text{cm}^2$ sample post annealing

Comparing the annealed and unannealed samples' reflection coefficient, it was noted that there was considerable variation in reflection coefficients of the samples with variation in dose of the dopants. As the doping increases reflection coefficient decreases, implying more waves pierce through the medium. But when the samples were annealed their reflection coefficient, irrespective of the dose, turned out to be the same, implying that the dose of the dopant at that point becomes irrelevant.

3.2 Simulation Results

The experimental setup was replicated, as shown in figure 11, in HFSS simulation software for each sample that has a different S11 plot. The height of coax cable picked for simulation

purpose was quarter wavelength. The waveguide and wafers dimensions were true to the actual size used for experiments.

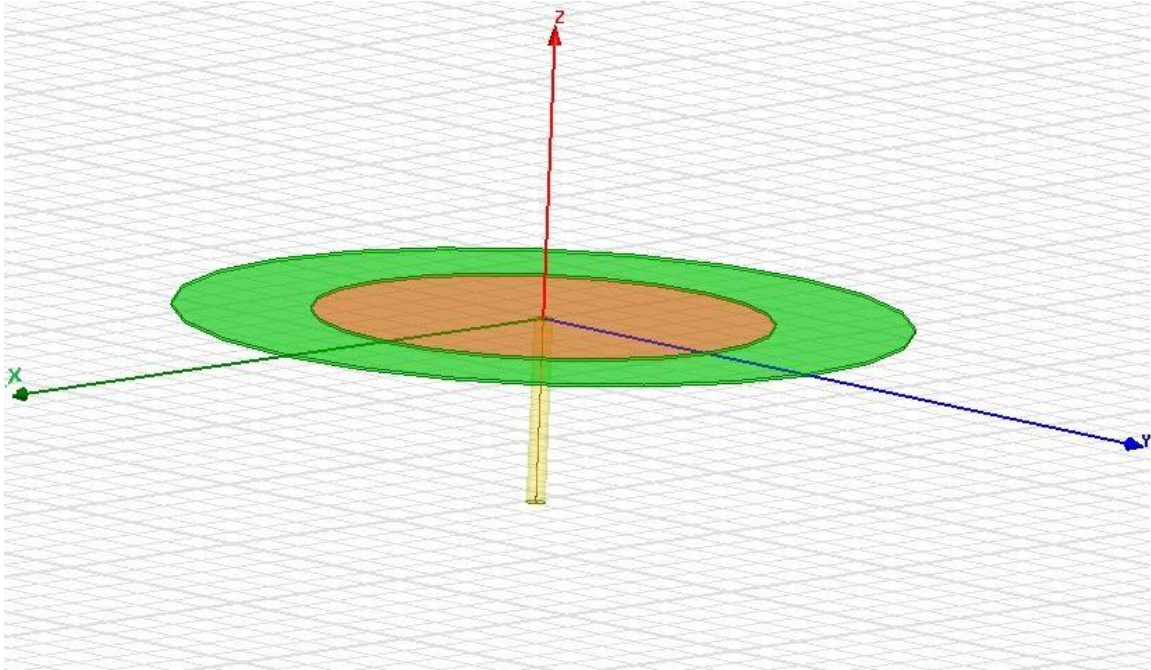


Figure 11 A model in HFSS replicating the experimental setup similar to the one shown in figure 2 and figure 3

Figure 12 shows simulation results for annealed samples, irrespective of dose since they all have same reflection coefficient implying same complex permittivity.

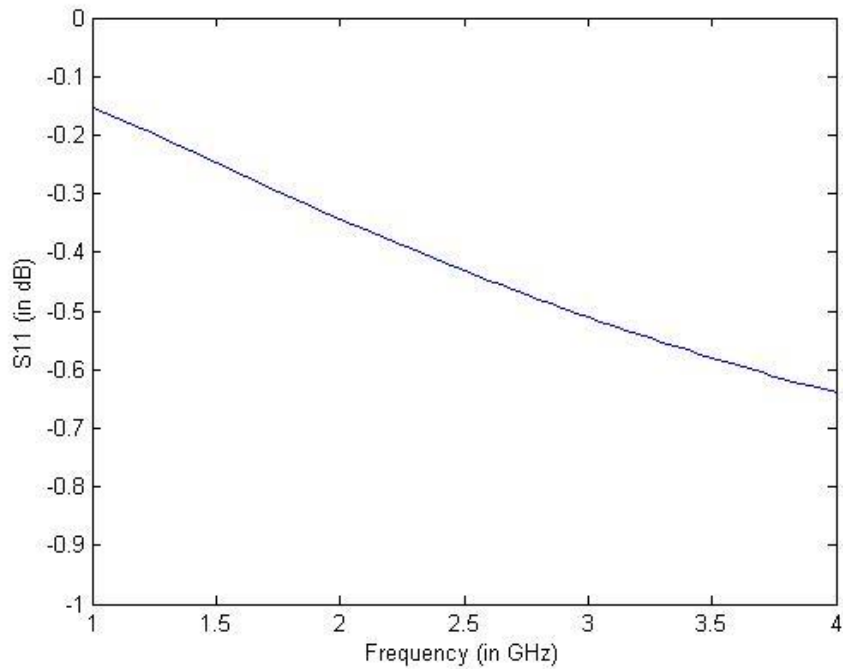


Figure 12 S11 in dB of annealed silicon wafer (of all dose) acquired from HFSS simulation

Figure 12 also represents the undoped sample's reflection coefficient prior to annealing. The reflection coefficient, obtained experimentally, for the undoped silicon before and after annealing was similar and hence it was safe to assume that the relative permittivity and the loss tangent was same. Figures 13-15 show doped silicon's reflection coefficient prior to annealing. The simulation was run in 2 batches. One from frequency 1-2 GHz and the other from 2-4 GHz, since the frequency range from 1-4 GHz was big and it was better to run the simulation in small intervals to get finer details.

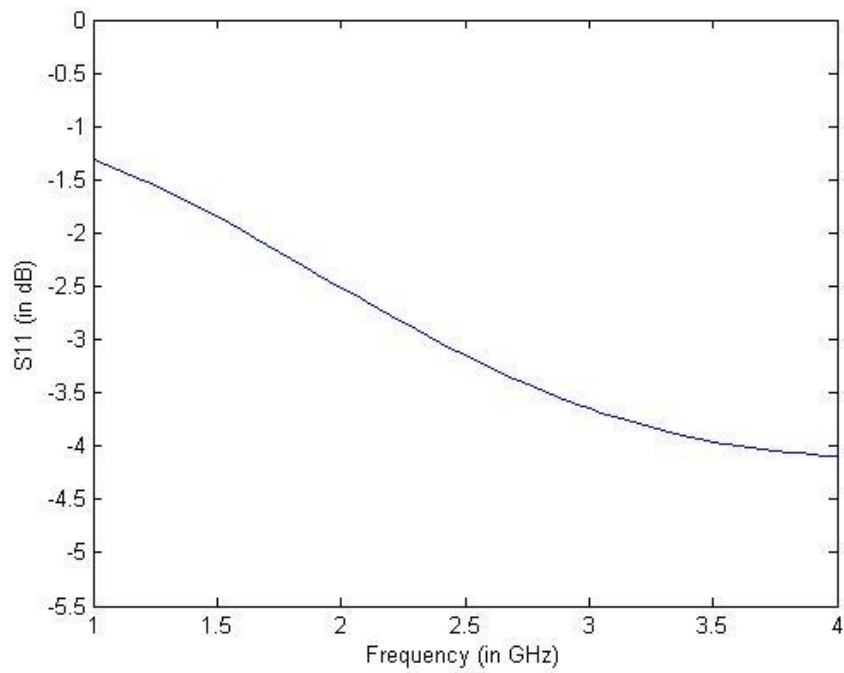


Figure 13 S11 in dB obtained via simulation for As doped Si unannealed sample with dose $1 \times 10^{15} / \text{cm}^2$

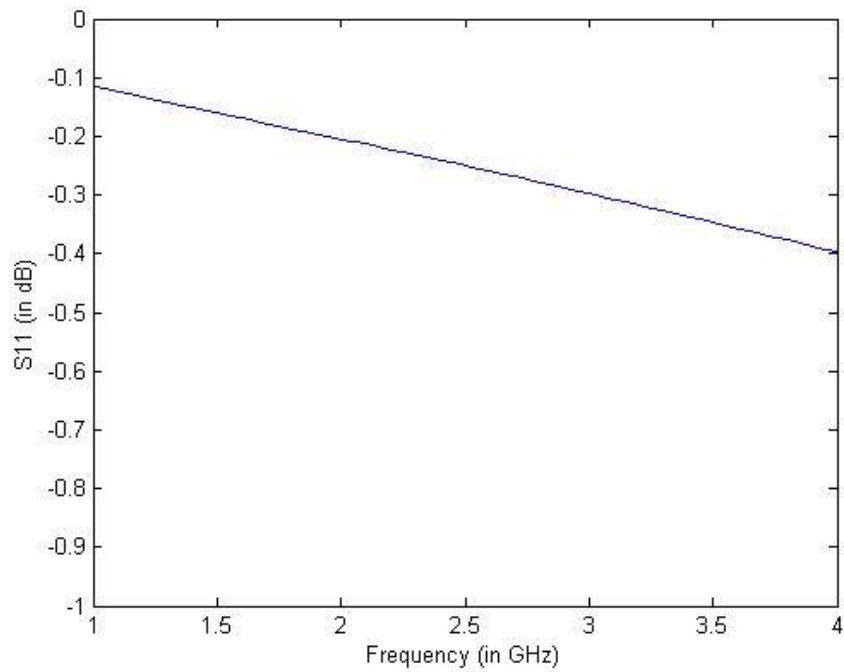


Figure 14 S11 in dB obtained via simulation for As doped Si unannealed sample with dose $2 \times 10^{15} / \text{cm}^2$

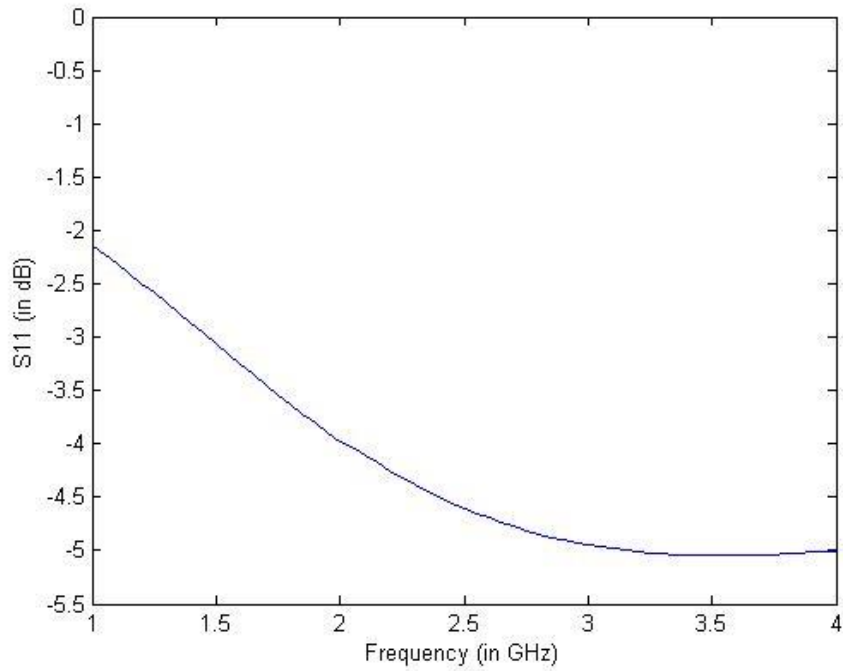


Figure 15 S11 in dB obtained via simulation for As doped Si unannealed sample with dose $4 \times 10^{15} / \text{cm}^2$

3.3 Analytical Results

Figure 16 shows the comparison between experimentally obtained reflection coefficients versus reflection coefficient acquired analytically for annealed samples.

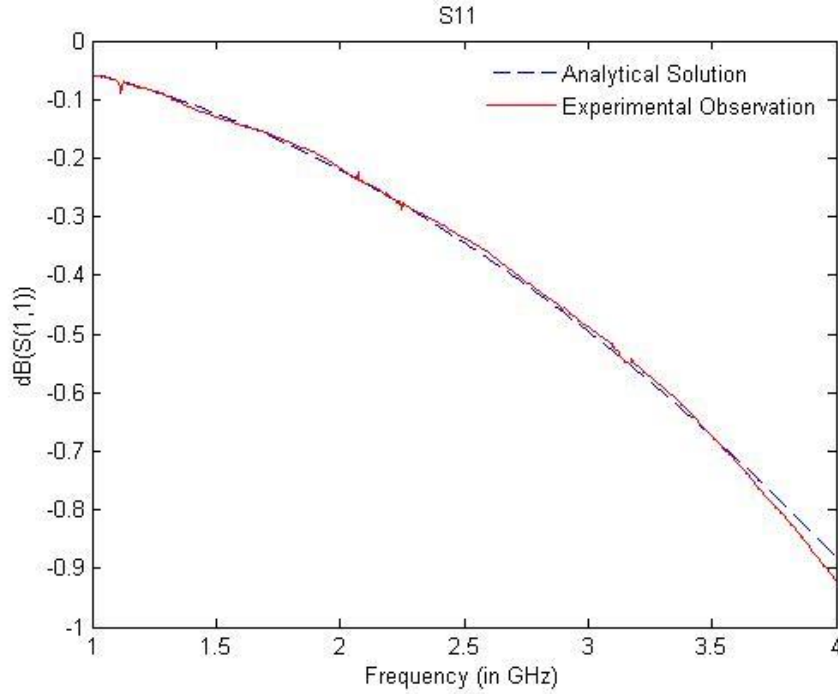


Figure 16 S11 (in dB) comparison of experimental results and analytical solution for annealed silicon samples (for all dose)

The analytical solution has 2 variables that was needed to trace the experimental curve, namely, relative permittivity and conductivity which is directly related to the loss tangent as shown in equation (3.1)

$$\tan \delta = \frac{\sigma}{\omega \epsilon} \quad (3.1)$$

3.4 Heating Curve

Study of heating curve for arsenic-implanted silicon wafer was proposed by Rajitha, *et al.* in [7]. The authors, in that paper, studied the heating curve in susceptor-assisted annealing process for a period of 240 seconds on arsenic-implanted silicon.

In this experiment, implanted samples were annealed for two different duration of time. First, the unannealed samples, for all doses, were annealed for 40 seconds and heating curve was recorded with the help of a low range pyrometer. Later, a new set of samples, for all doses, were annealed for 240 seconds and the heating curve was recorded with the help of a high range pyrometer. The low range pyrometer measures temperature upto 600 °C, whereas high range pyrometer measures temperature from 200 °C to 1200 °C. Figures 17-19 show the corresponding heating curve measured with the help of a low range pyrometer for 40 seconds.

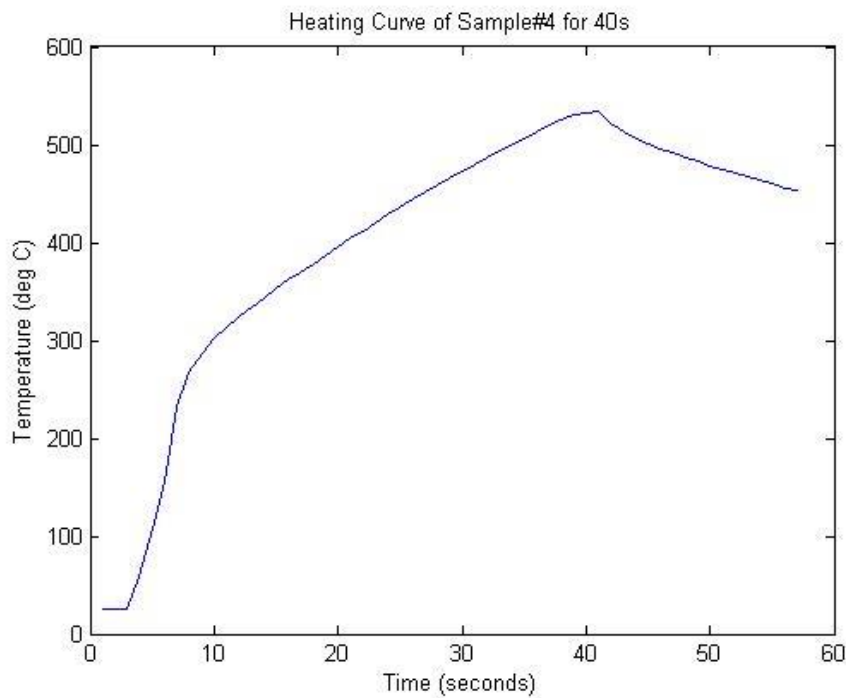


Figure 17 Heating curve of As doped Si with dose $1 \times 10^{15} / \text{cm}^2$

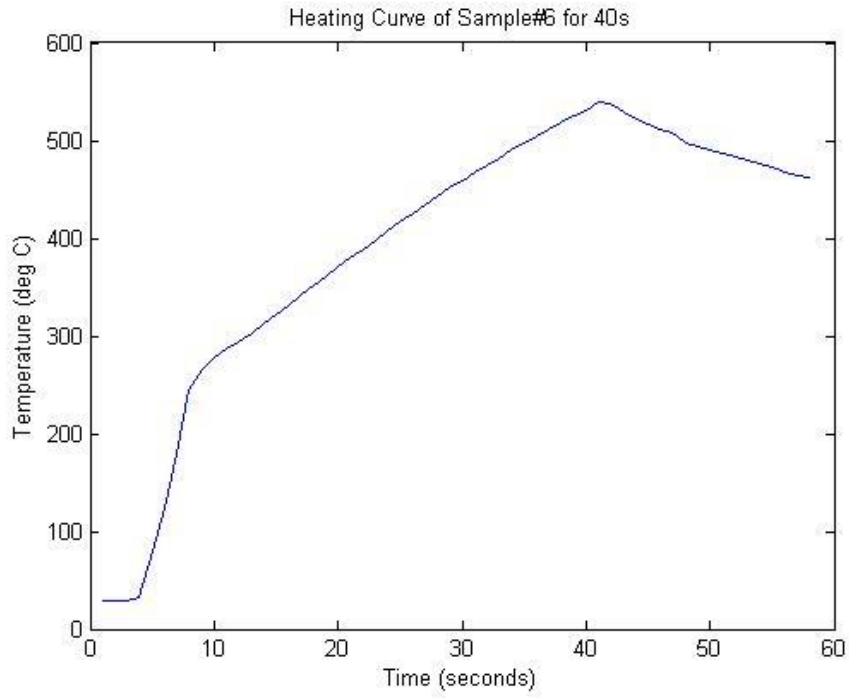


Figure 18 Heating curve of As doped Si with dose $2 \times 10^{15} / \text{cm}^2$

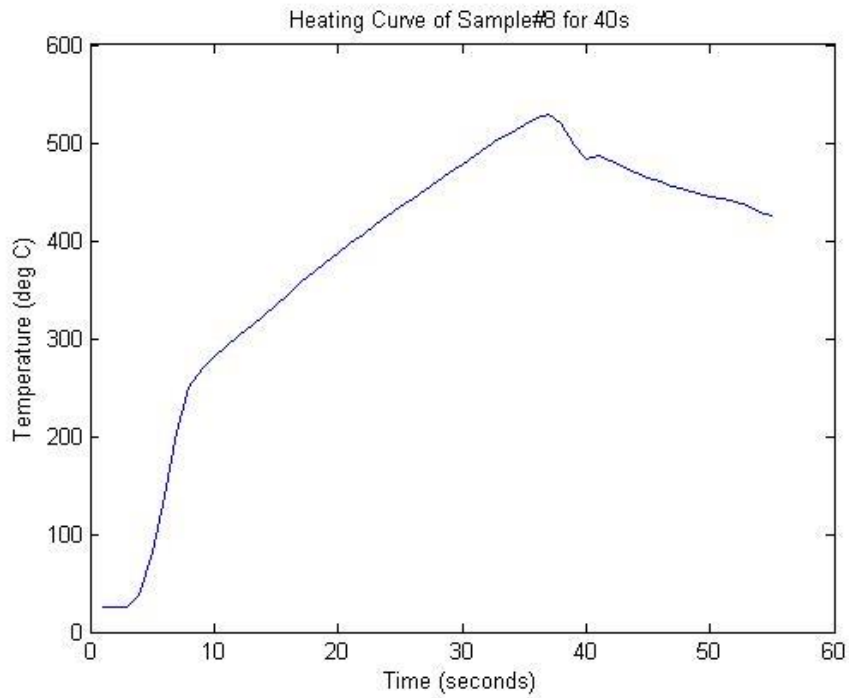


Figure 19 Heating curve of As doped Si with dose $4 \times 10^{15} / \text{cm}^2$

The heating curve during the susceptor-assisted annealing process, when done for 40 seconds, seem to increase exponentially at two different rates. Initially, the slope was steep but it tries to settle down later.

The other duration for susceptor-assisted annealing, to measure the heating curve, used was 240 seconds or 4 minutes using a high range pyrometer. Figures 20-22 show the heating curve obtained as a result.

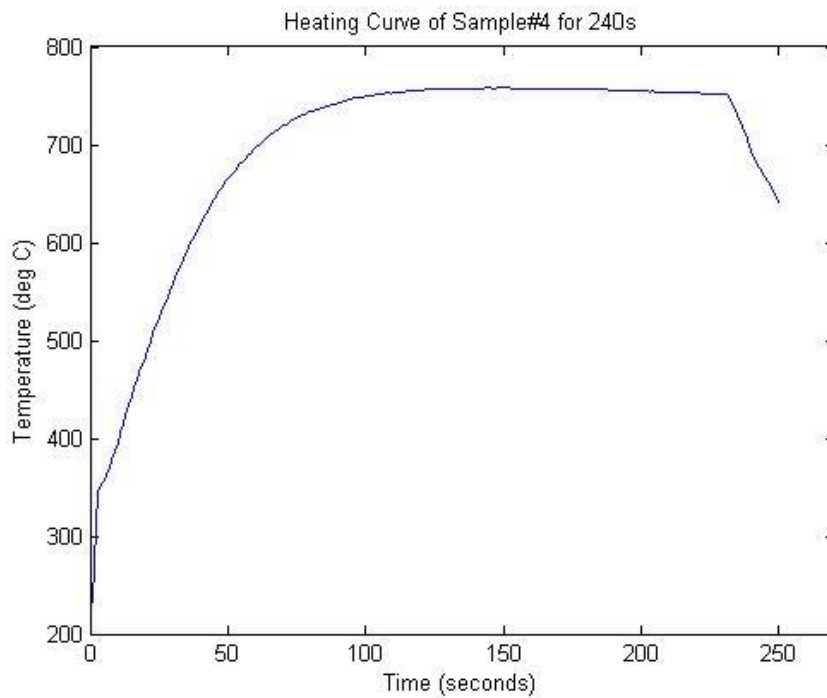


Figure 20 Heating curve of As doped Si with dose $1 \times 10^{15} / \text{cm}^2$

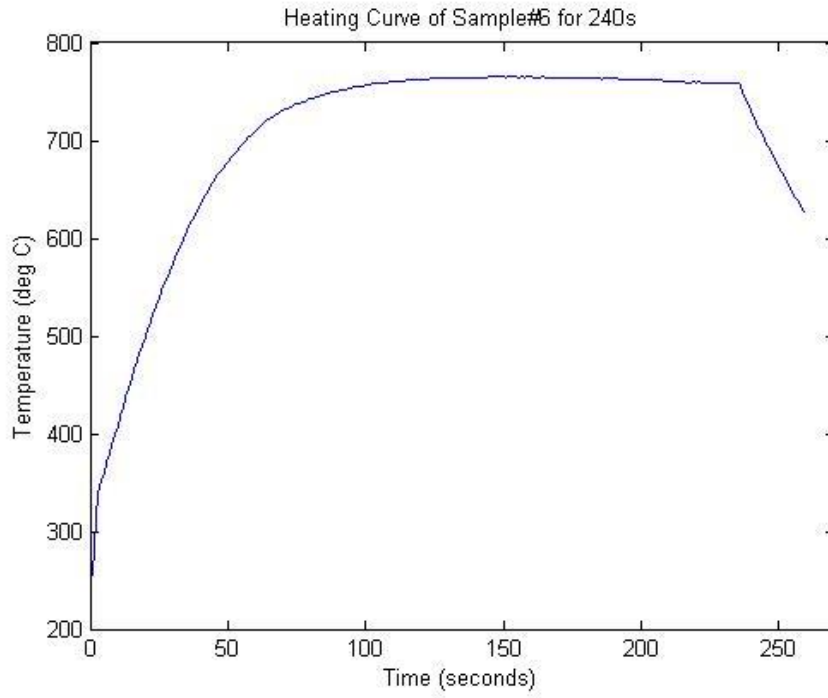


Figure 21 Heating curve of As doped Si with dose $2 \times 10^{15} / \text{cm}^2$

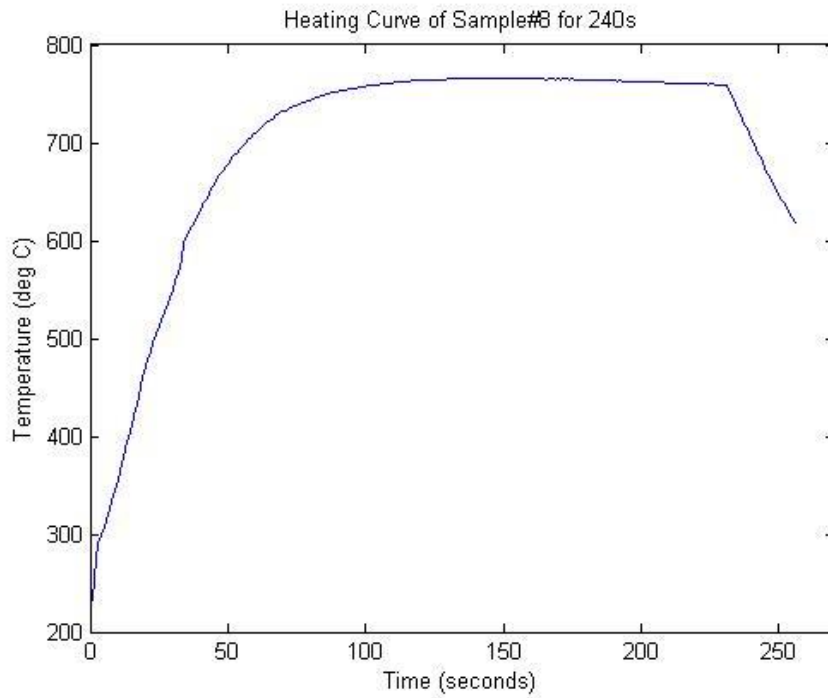


Figure 22 Heating curve of As doped Si with dose $4 \times 10^{15} / \text{cm}^2$

The trend was similar when the annealing process was carried out for 240 seconds, where the slope initially was steep but later it reduces and tried to settle down at a temperature near 750 °C. The exact temperature at which each sample settles, though, was different and as listed in Table 2.

| Dose (cm ⁻²) | Temperature (°C) |
|--------------------------|------------------|
| 1×10 ¹⁵ | 757 |
| 2×10 ¹⁵ | 772 |
| 4×10 ¹⁵ | 765 |

Table 2 Temperature at which arsenic-doped silicon attains stability for various dose

The temperature of the wafer doped with a dose of 2×10¹⁵ /cm² seems to settle at a higher temperature than expected to [2].

Figures 23 to 25 show heating curve of arsenic-doped silicon annealed with silicon as its base.

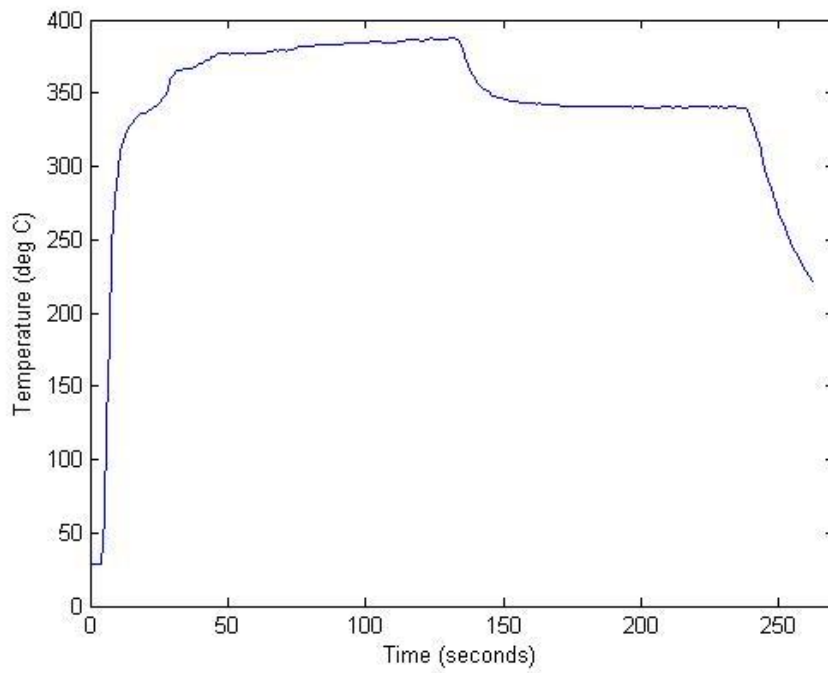


Figure 23 Heating curve of As doped Si with silicon base for dose $1 \times 10^{15} / \text{cm}^2$

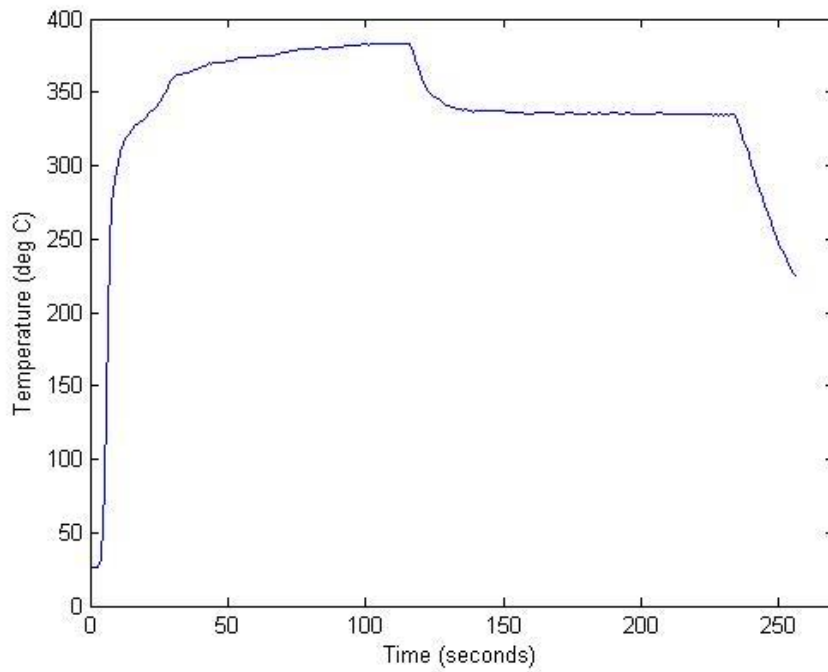


Figure 24 Heating curve of As doped Si with silicon base for dose $2 \times 10^{15} / \text{cm}^2$

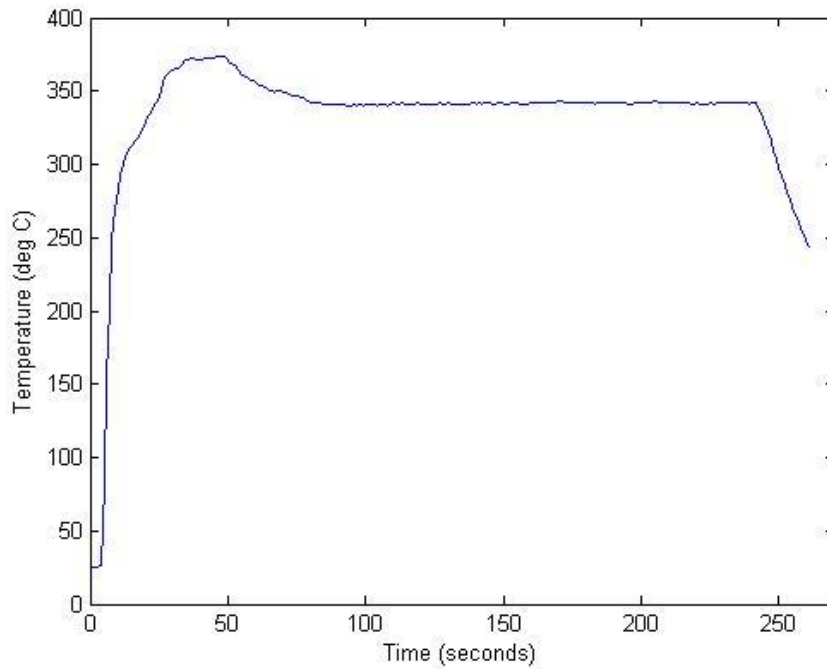


Figure 25 Heating curve of As doped Si with silicon base for dose $4 \times 10^{15} / \text{cm}^2$

The heating curve suggests that the temperature increases and stabilizes at a certain temperature, much below the susceptor-assisted annealing's stable temperature but after sometime it also reduced to stabilize at a different temperature, suggesting that the annealing process is complete. It also indicates that the temperature reached during annealing is not as high as seen in susceptor-assisted annealing.

CHAPTER 4
DISCUSSION

The complex permittivity of silicon wafer can be divided into two categories, relative permittivity, ϵ_r and loss tangent, $\tan\delta$. While the relative permittivity of the wafer remains constant throughout this experiment, loss tangent decreases with increase in dose for unannealed wafers, as noted from figures 5-7 and increases to a very large value when annealed, indicative of high conductivity of the material which is in accordance to the proposal by R. N. P. Vemuri, *et al* in [2]. Table 3 lists all the parameters that undergoes a change and also the parameters required for the conversion of absorbed microwave energy to heat energy.

| Sample# | Dose (cm ⁻²) | Relative Permittivity (dimensionless) | Loss Tangent (dimensionless) |
|---------|--------------------------|--|---------------------------------|
| 1 | 0 | 11.9 | 55.5 |
| 3 | 1×10 ¹⁵ | 11.9 | 5.0 |
| 5 | 2×10 ¹⁵ | 11.9 | 10.8 |
| 7 | 4×10 ¹⁵ | 11.9 | 4.8 |

Table 3 Unannealed sample's computed complex permittivity

The complex permittivity of the annealed samples, however, was the same irrespective of the dose. The relative permittivity was found to be 11.9 and the loss tangent to be 64.7. A deviation that was noticed was in the arsenic-doped sample with a dose 2×10¹⁵ /cm². The conductivity was found to be high in this case and does not follow the trend of other samples. This can be attributed either bad implantation or bad annealing. To confirm the

results obtained in this investigation, Hall measurements were done to the annealed samples and the results obtained were noted in Table 4.

| Dose (cm ⁻²) | Mobility (cm ² /V s) | Resistivity (Ω cm) | Concentration (cm ⁻³) |
|--------------------------|---------------------------------|----------------------|-----------------------------------|
| 1×10 ¹⁵ | 2.0×10 ⁻⁴ | 4.1×10 ² | -7.7×10 ¹⁹ |
| 2×10 ¹⁵ | 2.9×10 ² | 1.6×10 ⁻⁴ | -1.3×10 ²⁰ |
| 4×10 ¹⁵ | 2.5 | 3.6×10 ⁻³ | -6.8×10 ²⁰ |

Table 4 Hall measurement of Arsenic doped silicon post annealing

Table 4 suggests that the mobility and resistivity of sample with dose 2×10¹⁵ /cm² deviates from the accepted the value [7]. Ideally, the value should be somewhere in between the mobility and resistivity of the samples with dose 1×10¹⁵ /cm² and 4×10¹⁵ /cm², respectively.

Four-point-probe measurement was done on samples prior to annealing as well as post annealing. The four-point-probe contains four thin tungsten wires probes, collinearly placed, which were made to contact the sample. The voltage, V , was measured between the two inner probe, ideally without drawing any current, while the current, I , was made to flow through the two outer probes. Four-point-probe measurement gives V/I . Sheet resistant can be computed from this value by adding the correction factor, which varies depending on the shape and the size of the sample. Sheet resistance of the unannealed sample was negative, as was expected.

| Dose (cm ⁻²) | Sheet Resistance (Ω) |
|--------------------------|----------------------|
| 1 × 10 ¹⁵ | 127 |
| 2 × 10 ¹⁵ | 50.7 |
| 4 × 10 ¹⁵ | 37.8 |

Table 5 Four-point-probe measurement on samples conducted post annealing

The sheet resistance, evident from the Table 5, decreases with increase in dose, implying higher conductivity. As the dose of As⁺ increases, the slope of the heating curve reduces. It implies that it takes a longer time to reach the stability point for high dose material and rise in temperature much gradual, whereas in the case of lower dose, heating curve jumps to stability point quickly.

In [2], the authors proposed that the heating curves are influenced by the complex permittivity of the material and have proposed equation (4.1), to be the governing equation

$$\frac{\Delta T}{\Delta t} = \frac{\omega \epsilon_0 \epsilon_r \tan \delta |E|^2}{\rho_{mass} C_P} \quad (4.1)$$

where, $|E|^2$ is the magnitude of internal electric field, ρ_{mass} is mass density of the wafer and C_P is the heat capacity of the wafer, which was given to be 710 J/Kg-K for Si. Rate of change of temperature calculated from the heating curve and obtained by solving equation (4.1) and listed in Table 6, along with the rate of change of temperature from the heating curve calculated graphically during susceptor-assisted annealing and during annealing with silicon as base.

| Dose (cm ⁻²) | Rate of change of Temperature obtained from heating curve for susceptor-assisted annealing (K s ⁻¹) | Rate of change of Temperature obtained from heating curve with silicon base (K s ⁻¹) | Rate of change of temperature obtained analytically (K s ⁻¹) |
|-----------------------------|---|---|--|
| 1×10 ¹⁵ | 5.5 | 1.6 | 4.9×10 ⁻⁶ |
| 2×10 ¹⁵ | 5.4 | 1.9 | 11×10 ⁻⁶ |
| 4×10 ¹⁵ | 5.4 | 3.4 | 4.7×10 ⁻⁶ |

Table 6 Comparison of rate of change of temperature obtained analytically with the heating curve

The analytical solution indicates that the silicon is transparent to microwave radiation, which is more accurate in the case of intrinsic silicon. The damage is concentrated on the surface, until the skin depth, of the wafer and most of the bulk is intrinsic. The bulk properties of the sample does not affect the heating curve as seen from Table 6. The assumption made in [2], that for arsenic-doped silicon, the bulk complex permittivity has no effect and it is enough to know the sheet/surface properties of the material to characterize the heating curve during susceptor-assisted annealing process. Also, when the base is silicon the annealing process does not get to a very high temperature required for dopant activation and the rate of change of temperature is dose dependent, where as in susceptor-assisted annealing the rate of change is dose independent and reaches a very high temperature very quickly thereby activating the dopant simultaneously.

Two major assumptions made during this calculation was that the rate of change of temperature was linear as opposed to being exponential as noted from the observation and loss tangent was a constant value. Loss tangent varies with temperature [12], but the

variation was noted to be in between 5 and 65, neither of which would bring the calculated value close to the value obtained from graph, even for small intervals. Accurate measurements would still lead to the same inference. Hence, this approximation assumed was safe.

CHAPTER 5

CONCLUSION AND FUTURE WORK

The electrical properties of arsenic-doped silicon were calculated experimentally and corroborated with analytical analysis and simulation techniques. Two types of the samples were used for this investigation, one set was unannealed samples and the other was annealed. Heating curve, during the susceptor-assisted annealing and during annealing with silicon base, were observed and analyzed. It was shown that the bulk properties of arsenic-doped silicon has no effect on these heating curve and that it only depends on the sheet/surface property of the material.

The interesting study to follow this investigation is the study of capacitive heating of Si when sandwiched in between two susceptors. This study will help in analyzing the contribution of susceptors to the heating curve. This effect helps in characterizing the effect of wafer sitting in between the two susceptors

One peculiar finding from this experiment was that the sample with arsenic-doped silicon with dose $2 \times 10^{15} / \text{cm}^2$ was the most conductive, but this was attributed to inconsistency in either annealing process or during implantation.

REFERENCES

- [1] Y. Lee, F. Hsueh, S.Huang, J. Kowalski, A. Cheng, A. Koo, G.L.Luo, and C.Y.Wu, "A low-temperature microwave anneal process for boron-doped ultrathin Geepilayer on Si substrate", *IEEE Electron Dev. Lett.*, vol. 30, no. 2, pp. 123-125, 2009.
- [2] Rajitha N. P Vemuri, Mandar J. Gadre, N. D. Theodore, W. Chen, S. S. Lau and T. L. Alford, "Susceptor Assisted Microwave Annealing for Recrystallization and Dopant Activation of Arsenic Implanted Silicon", *Journal of Applied Physics*, vol.110 issue 3, pp. 034907-034907-7, 2011
- [3] Microwave Heating, 2014, [ONLINE], Available: <http://www.comsol.com/multiphysics/microwaveheating/>
- [4] Zhonghai Guo, Guangwen (George) Pan, Stephan Hall and Christopher Pan, "Broadband characterization of complex permittivity for low-loss dielectrics: circular PC broad disk approach," *IEEE Trans. on Antenna and Propagation*, vol. 57, no. 10, pp. 3126-3155, (October) 2009.
- [5] K. B. Keam and A. G. Williamson, " Analysis of a general coaxial-line/radial-line region junction", *IEEE Trans. on Microwave Theory and Techniques*, vol. 41, no. 3, pp. 516-520, (march) 1992
- [6] G. Williamson, "Analysis and modelling of a coaxial-line/rectangular waveguide junction," *IEEE Proc. H, Microwaves, Opt. Antennas*, vol. 129, no. 5, pp. 262-270, 198
- [7] Rajitha N. P. Vemuri, Mandar J. Gadre, N. D. Theodore and T. L. Alford, "Dopant Activation in Arsenic-Implanted Si by Susceptor-Assisted Low-Temperature Microwave Anneal", *IEEE Electron Device Letters*, vol. 32, no. 8, August 2011
- [8] J. W. Mayer and S. S. Lau, *Electronic Materials Science: For Integrated Circuits in Si and GaAs*, Macmillan, New York, 1990
- [9] Zhao Zhao, N. David Theodore, Rajitha N. P Vemuri, Wei Lu, S. S. Lau, A. Lanz and T. L. Alford, "Effective dopant activation by susceptor-assisted microwave annealing of low energy boron implanted and phosphorous implanted silicon," *Journal of Applied Phy.*, vol.114, no. 24, pp. 24903-24903-7, 2013

- [10] Constantine Balanis, "Advanced Electromagnetic Engineering," 2nd edition, John Wiley and sons Inc, 2012
- [11] W. H. Surber and G. E. Crouch, "Dielectric Measurement Methods for Solids at Microwave Frequencies," *Journal of Applied Physics*, vol. 19, (December) 1948, pp. 1130-1139
- [12] Jerzy Krupka, Jonathan Breeze, Anthony Centeno, Neil Alford, Thomas Claussen and Leif Jensen, "Measurements of Permittivity, Dielectric Loss Tangent and Resistivity of Float-Zone Silicon at Microwave Frequencies," *IEEE Transactions on Microwave Theory And Techniques*, vol. 54, no. 11, pp. 3995-4001 (November) 2006,
- [13] David M. Pozar, "Microwave Engineering," 4th edition, John Wiley and Sons Inc., 2012
- [14] D. Kajfez, W. P. Wheless Jr., and R. T. Ward, "Influence of an air gap on the measurement of dielectric constant by a parallel-plate dielectric resonator," *Proc. Inst. Elect. Eng.*, vol. 133, pt. H, no. 4, pp. 253-258, (August) 1986.
- [15] J. Baker-Jarvis, R. G. Geyer, and P. D. Domich, "A nonlinear least squares solution with causality constraints applied to transmission line permittivity and permeability determination," *IEEE Trans, Instrum. Meas.*, vol. 41, pp. 646-652, (October) 1992.
- [16] G. K. Gopalakrishnan and K. Chang, "Study of slits in microstrip ring resonators for microwave and optoelectronic applications," *Microwave Opt. Technol. Lett.*, vol. 5, no. 2, pp. 76
- [17] Y. Kobayashi and T. Senju, "Resonant modes in shielded uniaxial anisotropic dielectric rod resonators," *IEEE Trans. Microwave Theory Tech.*, vol. 41, pp. 2198-2205, (December) 1993.
- [18] J. Abdulnour, C. Akyel, and K.Wu, "A generic approach for permittivity measurement of dielectric materials using a discontinuity in a rectangular waveguide or a microstrip line," *IEEE Trans. Microwave Theory Tech.*, vol. 43, pp. 1060-1066, (May) 1995.
- [19] J. Krupka, K. Derzakowski, B. Riddle and J. Baker-Jarvis, "A dielectric resonator for measurements of complex permittivity of low loss dielectric materials as a

- function of temperature," *Measurement Science and Technology*, vol. 9, pp. 1751-1756, (October) 1998
- [20] J. Krupka, K. Derzakowski, A. Abramowicz, M. Tobar, and R. G. Geyer "Whispering gallery modes for complex permittivity measurements of ultra-low loss dielectric materials," *IEEE Trans. on Microwave Theory Tech*, vol. MTT-47, pp. 752-759, (June) 1999.
- [21] J. Krupka, K. Derzakowski, M.E. Tobar, J. Hartnett, and R.G. Geyer, "Complex permittivity of some ultralow loss dielectric crystals at cryogenic temperatures," *Measurement Science and Technology*, vol. 10, pp. 387-392, (October) 1999.
- [22] Byoungjoong Kang, Jaiwon Cho, " Nondestructive measurement of complex permittivity and permeability using multilayered coplanar waveguide structures," *IEEE Microwave and Wireless Components Letters*, vol. 15, no. 5, (May) 2005
- [23] Xiang Yi Fangl, David Linton, " Non-destructive characterization for dielectric loss of low permittivity substrate materials," *Measurement Science and Technology*, 15 747C75 112, 2004
- [24] Janezic M.D., Kuester E.F., Baker-Jarvis J., "Broadband complex permittivity measurements of dielectric substrates using a split-cylinder resonator," *IEEE MTT-S International Microwave Symposium Digest*, pp. 1817-1820, Fort Worth, (June) 2004.
- [25] Janezic M.D., "Nondestructive relative permittivity and Loss tangent measurements using a split-cylinder resonator, "Ph.D. Thesis, University of Colorado, 2003.
- [26] Misra D. K., "A quasi-static analysis of open-end coaxial lines," *IEEE Trans Microwave Theory Tech*. 35 925-8, 1987
- [27] Misra D. K., "On the measurement of the complex permittivity of materials by an open-end coaxial probe," *IEEE Microw. Guid. Wave Lett*. 5 161-3, 1995
- [28] P. K. Singh et al., "High frequency measurement of dielectric thin films," *IEEE MTTs Int. Microwave Symp. Dig.*, San Diego, CA, pp. 1457-1460, (May) 1994

- [29] W. Williamson III et al., "High frequency dielectric properties of thin film PZT capacitors," *Integrated Ferroelectrics*, vol. 10, pp. 335-342, 1995.
- [30] Robert H. Voelker, Guang-Wen Pan,"Determination of complex permittivity of low- Loss dielectrics," *IEEE Trans. Microwave Theory Tech.*, vol. 45, no. 10, (October) 1997